

# Dirac Theory and Topological Phases of Silicon Nanotube

Motohiko Ezawa

Department of Applied Physics, University of Tokyo, Hongo 7-3-1, 113-8656, Japan

Silicon nanotube is constructed by rolling up a silicene, i.e., a monolayer of silicon atoms forming a two-dimensional honeycomb lattice. It is a semiconductor or an insulator owing to relatively large spin-orbit interactions induced by its buckled structure. The key observation is that this buckled structure allows us to control the band structure by applying electric field  $E_z$ . When  $E_z$  is larger than a certain critical value  $E_{cr}$ , by analyzing the band structure and also on the basis of the effective Dirac theory, we demonstrate the emergence of four helical zero-energy modes propagating along nanotube. Accordingly, a silicon nanotube contains three regions, namely, a topological insulator, a band insulator and a metallic region separating these two types of insulators. The wave function of each zero mode is localized within the metallic region, which may be used as a quantum wire to transport spin currents in future spintronics. We present an analytic expression of the wave function for each helical zero mode. These results are applicable also to germanium nanotube.

## INTRODUCTION

Carbon nanotube is one of the most fascinating materials. There is a variety of nanotubes from metal to insulator depending on how it is constructed by rolling up a graphene[1, 2]. Similarly, silicon nanotube may be constructed by rolling up a silicene[3–6], a monolayer of silicon atoms forming a two-dimensional honeycomb lattice. Silicon nanotubes have already been manufactured[7–9]. Almost every striking property of carbon nanotube is expected to be transferred to this innovative material since carbon and silicon belong to the same family in the periodic table. Nevertheless there exists a major difference. A large ionic radius of silicon induces a buckled structure[5], which results in a relatively large spin-orbit (SO) gap of 1.55meV. Accordingly, silicon nanotube has a finite gap and it is always a semiconductor or an insulator. One might think it is an ordinary band insulator just as most carbon nanotubes are. See Fig.1 for an illustration of carbon nanotube and silicon nanotube.

In this paper we reveal an amazing property of silicon nanotube thanks to this buckled structure when it is placed in external electric field. Analyzing the band structure in the presence of electric field  $E_z$  perpendicular to the nanotube axis, we demonstrate that silicon nanotube is actually a topological insulator. When  $E_z$  is beyond a certain critical field  $E_{cr}$ , we find four zero-energy modes to emerge in the bulk band gap and form metallic regions along a nanotube. A silicon nanotube is made of three different phases, the topological insulator region, the bulk insulator region and the metallic region separating them.

Topological insulator[10, 11] is a new state of quantum matter characterized by a full insulating gap in the bulk and gapless edges topologically protected. These states are made possible due to the combination of the SO interaction and the time-reversal symmetry. The two-dimensional topological insulator is a quantum spin Hall (QSH) insulator with helical gapless edge modes[12], which is a close cousin of the integer quantum Hall state. QSH insulator was proposed by Kane and Mele in graphene[13]. However, since the SO gap is rather weak in graphene, the QSH effect can occur in graphene only

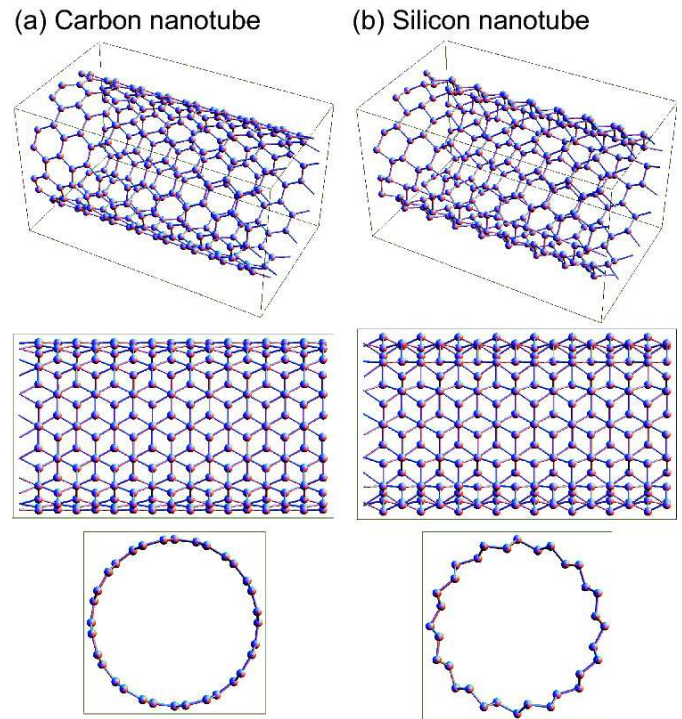


FIG. 1: (a) Carbon nanotube and (b) silicon nanotube. The lattice is distorted due to a large ionic radius of a silicon atom and forms a buckled structure in silicon nanotube.

at unrealistically low temperature[14, 15]. Our finding is that it is materialized naturally in silicon nanotube.

As we have stated, there emerge four zero-energy modes in silicon nanotube under uniform electric field. They are helical edge modes of a topological insulator and propagate along a nanotube: They transport only spins without charges. These observations are supported by the effective Dirac theory. We construct explicitly the wave functions describing the four helical zero modes. In conclusion, we are able to realize a dissipationless spin current along a silicon nanotube by applying uniform electric field. It may be used as a quantum wire in future spintronics.

## SILICENE AND TIGHT-BINDING MODEL

The band structure of a silicon nanotube is obtained simply by imposing a certain periodic boundary condition to a silicene sheet provided the diameter is large enough. Silicene consists of a honeycomb lattice of silicon atoms with two sublattices made of A sites and B sites. The states near the Fermi energy are  $\pi$  orbitals residing near the K and K' points at opposite corners of the hexagonal Brillouin zone. We refer to the K or K' point also as the  $K_\eta$  point with the valley index  $\eta = \pm 1$ . Due to the buckled structure the two sublattice planes are separated by a distance, which we denote by  $2\ell$  with  $\ell = 0.23\text{\AA}$ . It generates a staggered sublattice potential  $\propto 2\ell E_z(x, y)$  between silicon atoms at A sites and B sites in external electric field  $E_z(x, y)$ .

The silicene system is described by the four-band second-nearest-neighbor tight binding model[16],

$$\begin{aligned}
H = & -t \sum_{\langle i, j \rangle \alpha} c_{i\alpha}^\dagger c_{j\alpha} + i \frac{\lambda_{\text{SO}}}{3\sqrt{3}} \sum_{\langle\langle i, j \rangle\rangle \alpha\beta} \nu_{ij} c_{i\alpha}^\dagger \sigma_{\alpha\beta}^z c_{j\beta} \\
& - i \frac{2}{3} \lambda_{\text{R}} \sum_{\langle\langle i, j \rangle\rangle \alpha\beta} \mu_i c_{i\alpha}^\dagger \left( \boldsymbol{\sigma} \times \hat{\mathbf{d}}_{ij} \right)_{\alpha\beta}^z c_{j\beta} \\
& + \ell \sum_{i\alpha} \mu_i E_z c_{i\alpha}^\dagger c_{i\alpha}, \tag{1}
\end{aligned}$$

where  $c_{i\alpha}^\dagger$  creates an electron with spin polarization  $\alpha$  at site  $i$ , and  $\langle i, j \rangle / \langle\langle i, j \rangle\rangle$  run over all the nearest/next-nearest neighbor hopping sites. The first term represents the usual nearest-neighbor hopping with the transfer energy  $t = 1.6\text{eV}$ . The second term represents the effective SO coupling with  $\lambda_{\text{SO}} = 3.9\text{meV}$ , where  $\boldsymbol{\sigma} = (\sigma_x, \sigma_y, \sigma_z)$  is the Pauli matrix of spin,  $\nu_{ij} = (\mathbf{d}_i \times \mathbf{d}_j) / |\mathbf{d}_i \times \mathbf{d}_j|$  with  $\mathbf{d}_i$  and  $\mathbf{d}_j$  the two bonds connecting the next-nearest neighbors. The third term represents the Rashba SO coupling with  $\lambda_{\text{R}} = 0.7\text{meV}$ , where  $\mu_i = \pm 1$  for the A (B) site, and  $\hat{\mathbf{d}}_{ij} = \mathbf{d}_{ij} / |\mathbf{d}_{ij}|$ . The fourth term is the staggered sublattice potential term. The same Hamiltonian as can be used to describe germanene, which is a honeycomb structure of germanium[5, 16], where various parameters are  $t = 1.3\text{eV}$ ,  $\lambda_{\text{SO}} = 43\text{meV}$ ,  $\lambda_{\text{R}} = 10.7\text{meV}$  and  $\ell = 0.33\text{\AA}$ .

By diagonalizing the Hamiltonian (1) under uniform electric field  $E_z$ , the band gap  $\Delta(E_z)$  of silicene is determined to be

$$\Delta(E_z) = 2|\ell E_z - \eta s_z \lambda_{\text{SO}}| \tag{2}$$

at the  $K_\eta$  point, where  $s_z = \pm 1$  is the electron spin. The gap  $\Delta(E_z)$  closes at  $E_z = \eta s_z E_c$  with

$$E_c = \lambda_{\text{SO}} / \ell = 17\text{meV}/\text{\AA}, \tag{3}$$

where it is a semimetal due to gapless modes. It has been shown[6] that silicene is a topological insulator for  $|E_z| < E_c$ , while it is a bulk insulator for  $|E_z| > E_c$ , as illustrated

in Fig.2. Hence a topological phase transition occurs between a topological insulator and a band insulator as  $E_z$  changes.

The topological insulator is characterized by one of the following two defining properties[10, 11]. (1) The topological insulator has a nontrivial topological number, the  $\mathbb{Z}_2$  index[13], which is defined only for a gapped state. (2) There emerge gapless modes in the edges [Fig.2(b)]. These two properties are closely related one to another. Indeed, the reason why gapless modes appear in the edge of a topological insulator is understood as follows. When a topological insulator has an edge beyond which the region has the trivial  $\mathbb{Z}_2$  index, the band must close and yield gapless modes in the interface. Otherwise the  $\mathbb{Z}_2$  index cannot change its value across the interface.

The above criteria cannot be applicable to a nanotube as they are since it is intrinsically one-dimensional (1D). We overcome the problem by applying electric field and by creating a domain with 1D edges in the surface of a nanotube: See Fig.5 we derive later.

## SILICON NANOTUBE

A silicon nanotube can be constructed by rolling up a silicene precisely just as a carbon nanotube is constructed by rolling up a graphene[1, 2]. There are a variety of ways how to rolling up a silicene as in the case of carbon nanotubes. It is specified by the chiral vector,

$$\mathbf{L} = n_1 \mathbf{a}_1 + n_2 \mathbf{a}_2, \tag{4}$$

where  $\mathbf{a}_1$  and  $\mathbf{a}_2$  are the basis vectors of the honeycomb lattice with integers  $n_1$  and  $n_2$ . Let us take the coordinate  $(x, y)$  with the  $x$ -axis parallel to the chiral vector  $\mathbf{L}$  (the circumference direction) and the  $y$ -axis orthogonal to it (the nanotube axis direction). The nanotube's circumference is given by

$$L = |\mathbf{L}| = a \sqrt{n_1^2 + n_2^2 - n_1 n_2}, \tag{5}$$

where  $a = 3.86\text{\AA}$  is the lattice constant. Let us denote the conjugate momentum as  $(\hbar k_x, \hbar k_y)$ . We impose the periodic boundary condition  $\psi(x+L, y) = \psi(x, y)$ . It makes the wave vector  $k_x$  discrete, i.e.,

$$k_x = 2\pi j / L, \quad j = 0, 1, \dots, 2n - 1, \tag{6}$$

where  $2n$  is the number of silicon atoms per unit cell. The wave vector  $k_y$  remains continuous within the 1D first Brillouin zone,

$$-\pi/T \leq k_y \leq \pi/T, \tag{7}$$

where  $T$  is the length of the primitive translation vector in the  $y$  direction. The 1D energy bands are given by the straight lines specified by (6) and (7) in the  $(k_x, k_y)$  space. The simplest nanotube is the armchair type, where  $L = \sqrt{3}na$ .

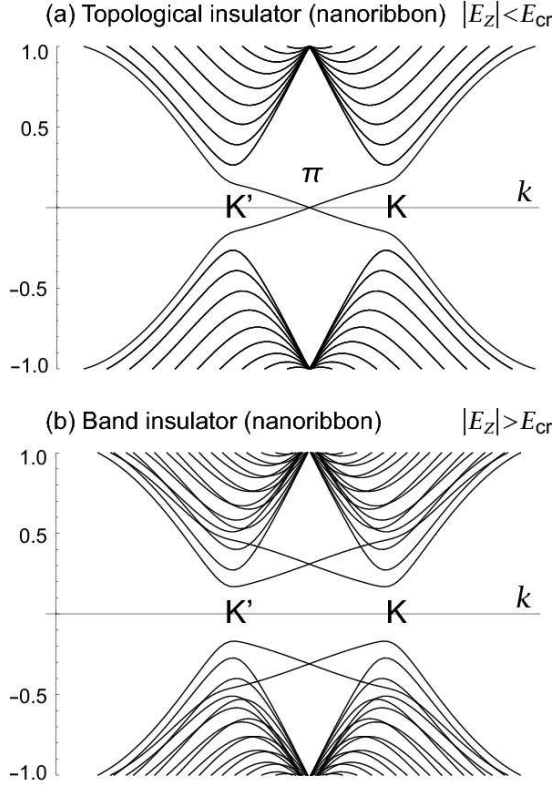


FIG. 2: (Color online) (a) The band structure of silicene nanoribbon for  $|E_z| < E_{cr}$ . There appear two bands crossing the gap since there are two edges, indicating it is topological insulator. When the Rashba interaction is neglected ( $\lambda_R = 0$ ), each band contains two-fold degenerate zero-energy states corresponding to up and down spins. (b) The band structure of silicene nanoribbon for  $|E_z| > E_{cr}$ . All states are gapped, and it is bulk insulator. The horizontal axis is the momentum, and the vertical axis is the energy in unit of the transfer energy  $t$ .

The energy spectrum of a silicon nanotube is simply given by

$$E_j(k_y) = \mathcal{E}(k_x, k_y), \quad (8)$$

in terms of the energy spectrum  $\mathcal{E}(k_x, k_y)$  of silicene. The energy spectrum of a carbon nanotube can be gapless since graphene has a gapless band. There is a variety of carbon nanotubes from metal to insulator depending on the way how to choose the chiral vector  $\mathbf{L}$ . On the contrary, a silicon nanotube has always a finite gap since silicene has a finite gap. The band gap is rather insensitive to the choice of  $\mathbf{L}$ .

We have calculated the band structure of an armchair silicon nanotube based on the tight-binding model (1) by changing the uniform external electric field  $E_z$ . The band structure is strikingly different for  $|E_z| < E_{cr}$  and  $|E_z| > E_{cr}$ , as illustrated in Fig.3. All states are gapped for  $|E_z| < E_{cr}$ . On the other hand, for  $|E_z| > E_{cr}$ , there appear four bands crossing the gap at the K and K' points. When the Rashba interaction is neglected ( $\lambda_R = 0$ ), each band contains two-fold degenerate zero-energy states corresponding to up and down spins. Even

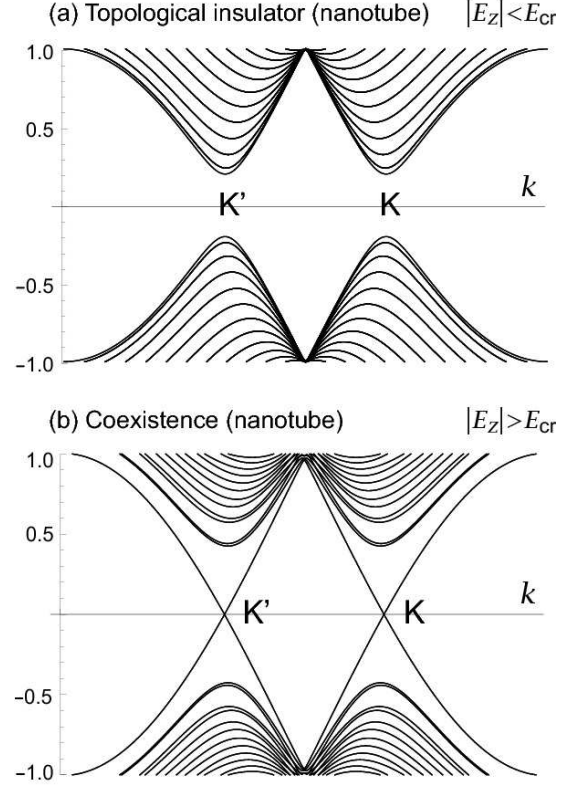


FIG. 3: (Color online) (a) The band structure of silicon nanotube for  $|E_z| < E_{cr}$ . All states are gapped, and it is topological insulator. (b) The band structure of silicon nanotube for  $|E_z| > E_{cr}$ . There appear four bands crossing the gap. They are the zero-energy states separating the topological and band insulating states in the nanotube surface: See Fig.5. When the Rashba interaction is neglected ( $\lambda_R = 0$ ), each band contains two-fold degenerate zero-energy states corresponding to up and down spins. The horizontal axis is the momentum, and the vertical axis is the energy in unit of the transfer energy  $t$ .

when  $\lambda_R \neq 0$ , the degeneracy remains unsolved at the K (K') point, though it is slightly resolved away from these points. The feature of the zero-energy states is highly contrasted with that in a silicene nanoribbon, where they emerge at  $k = \pi$  as in Fig.2(a).

We show the probability density of these four zero modes in Fig.4, to which we have assigned the spin  $s_z$  and the valley  $K_\mu$  where they appear. We are able to make the assignment and determine the direction of the current based on the effective Dirac theory: See a sentence below (17) and Fig.5. Here we explain them by using the gap formula (2) and the band structure in Fig.3(b).

It follows from the formula (2) that the electrons with spin  $s_z = \pm 1$  are gapless at the  $K_\pm$  point for  $E_z > 0$  and that the electrons with spin  $s_z = \mp 1$  are gapless at the  $K_\pm$  point for  $E_z < 0$ . Thus the peaks indexed by  $K\uparrow$  appear in the upper half and those indexed by  $K\downarrow$  appear in the lower half of the nanotube. Recall that  $E_z$  is the electric field between the A and B sublattices, which is opposite between the upper and lower halves of the nanotube. Furthermore, the direc-

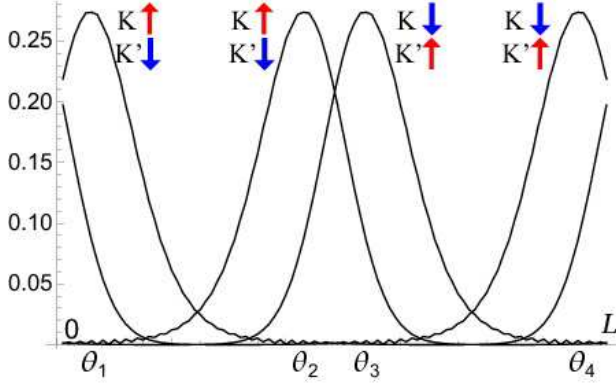


FIG. 4: (Color online) The probability density of the zero modes in silicon nanotube. There appear four peaks at  $\theta = \theta_j$ , with  $\sin \theta_j = \pm E_{\text{cr}}/E$ , as indicates the emergence of four metallic states separating topological and band insulators: See Fig.5. The horizontal axis is the circumference ( $0 < x < L$ ) or the angle ( $0 < \theta < 2\pi$ ).

tion of the current can be determined by examining the dispersion relation of the zero-energy mode in the band structure [Fig.3(b)]. We find the up-spin electrons and the down-spin electrons propagate into the opposite directions in each peak. Namely the current is helical, that is, it is a spin current, as illustrated in Fig.5. It is a characteristic feature that helical zero modes appear along the edge of a topological insulator. We conclude that the zero-energy metallic state separates the topological and band insulating states in a silicon nanotube.

### DIRAC THEORY

In order to explore deeper physics of the helical zero modes, we analyze the low-energy effective Hamiltonian derived from the tight binding model (1). It is described by the Dirac theory around the  $K_\eta$  point as[16]

$$H_\eta = \hbar v_F (k_x \tau_x - \eta k_y \tau_y) + \eta \tau_z h_{11} + \ell E_z \tau_z, \quad (9)$$

with

$$h_{11} = -\lambda_{\text{SO}} \sigma_z - a \lambda_{\text{R}} (k_y \sigma_x - k_x \sigma_y), \quad (10)$$

where  $\tau_a$  is the Pauli matrix of the sublattice pseudospin,  $v_F = \frac{\sqrt{3}}{2} a t = 5.5 \times 10^5 \text{ m/s}$  is the Fermi velocity.

We have shown numerically that there emerge four zero-energy states inside the bulk band gap as in Fig.3(b). The low-energy Dirac theory allows us to investigate analytically the properties of these helical zero modes. In so doing we set  $\lambda_{\text{R}} = 0$  to simplify calculations. This approximation is justified by the following reasons. First all all, we have numerically checked that the band structure is rather insensitive to  $\lambda_{\text{R}}$  based on the tight-binding Hamiltonian (1). Second,  $\lambda_{\text{R}}$  appears only in the combination  $(k_x \pm i k_y) \lambda_{\text{R}}$  in the Hamiltonian (9), which vanishes exactly at the  $K_\pm$  points. Third, the critical electric field  $E_{\text{cr}}$  is independent of  $\lambda_{\text{R}}$  as in (3).

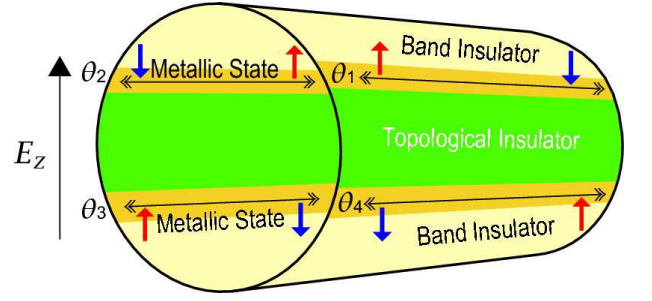


FIG. 5: (Color online) An illustration of silicon nanotube under electric field  $E > E_{\text{cr}}$ . There appear two topological insulator regions and two band insulator regions. They are separated by metallic states made of helical zero modes. A spin current flows in each metallic region as indicated. For instance, up-spin (down-spin) electrons propagate into the left (right) direction at  $\theta = \theta_1$ .

We take the  $y$ -axis parallel to the nanotube axis and the  $x$ -axis along the circumference. We may set  $k_y = \text{constant}$  due to the translational invariance along the  $y$  axis. The momentum  $k_y$  is a good quantum number. Setting

$$\Psi(x, y) = e^{i k_y y} \Phi(x), \quad (11)$$

we seek the zero-energy solution, where  $\Psi(x, y)$  is a four-component amplitude. The particle-hole symmetry guarantees the existence of zero-energy solutions satisfying the relation  $\phi_B(x) = i \xi \phi_A(x)$  with  $\xi = \pm 1$ . Here,  $\phi_A$  is a two-component amplitude with the up spin and the down spin,  $\phi_A = (\phi_A^+, \phi_A^-)^t$ . Then the eigenvalue problem yields

$$H_\eta \phi_A(x) = E_{\eta \xi} \phi_A(x), \quad (12)$$

together with a linear dispersion relation

$$E_{\eta \xi} = \eta \xi \hbar v_F k_y. \quad (13)$$

The equation of motion for the component  $\phi_A^{s_z}(x)$  reads

$$(\xi \hbar v_F \partial_x + \eta s_z \lambda_{\text{SO}} - \ell E_z(x)) \phi_A^{s_z}(x) = 0. \quad (14)$$

We apply the uniform electric field  $E$  perpendicular to the nanotube axis.

The effective field for electrons in a silicon nanotube is given by

$$E_z(x) = E \sin \theta \quad (15)$$

with  $\theta = 2\pi x/L$ . We take  $E > E_{\text{cr}}$  with (3). We solve the equation

$$E_z(\theta) = \eta s_z E_{\text{cr}}. \quad (16)$$

Let us chose one solution and denote it as

$$\theta_{\text{cr}} = \text{Arcsin}(E_{\text{cr}}/E). \quad (17)$$

We obtain two solutions  $\theta_1 = \theta_{\text{cr}}$  and  $\theta_2 = \pi - \theta_{\text{cr}}$  for  $\eta s_z = +1$ , and two solutions  $\theta_3 = \pi + \theta_{\text{cr}}$  and  $\theta_4 = 2\pi - \theta_{\text{cr}}$  for

$\eta s_z = -1$ . It implies that the zero modes at  $\theta = \theta_1$  contains up-spin electrons ( $s_z = +1$ ) from the K valley ( $\eta = +1$ ) and down-spin electron ( $s_z = -1$ ) from the K' valley ( $\eta = -1$ ), and so on, as illustrated in Fig.4. As we shall soon see, the sign  $\xi$  is fixed at each  $\theta_j$ , as implies that up-spin and down spin electrons propagate into the opposite directions according to the dispersion relation (13). The current is helical, whose direction is determined by the sign of  $\xi$ .

The equation of motion (14) is rewritten as

$$\left( \frac{2\pi}{L} \xi \hbar v_F \partial_\theta - 2\ell E \cos \frac{\theta + \theta_j}{2} \sin \frac{\theta - \theta_j}{2} \right) \phi_A^{s_z}(\theta) = 0. \quad (18)$$

To construct the solution near  $\theta_j$ , we approximate

$$\cos \frac{\theta + \theta_j}{2} \simeq \cos \theta_j. \quad (19)$$

We can explicitly solve this as

$$\phi_A^{s_z}(\theta) = C \exp \left[ -\xi \frac{2L\ell E}{\pi \hbar v_F} \cos \theta_j \cos \frac{\theta - \theta_j}{2} \right], \quad (20)$$

where  $C$  is the normalization constant. It satisfies the periodic boundary condition  $\phi_A(\theta + \pi) = \phi_A(\theta)$  or  $\phi_A(x + L) = \phi_A(x)$ . The sign  $\xi$  is to be chosen so as to make the peak of the wave function to appear at  $\theta = \theta_j$ , and we have

$$\phi_A^{s_z}(\theta) = C \exp \left[ \frac{2L\ell E}{\pi \hbar v_F} |\cos \theta_j| \cos \frac{\theta - \theta_j}{2} \right], \quad (21)$$

We obtain  $\xi = -1$  at  $\theta = \theta_1$  and  $\theta = \theta_4$ , while  $\xi = +1$  at  $\theta = \theta_2$  and  $\theta = \theta_3$ . As we have noticed in the sentence below (17), the sign of  $\xi$  determines the direction of the helical current at each  $\theta_j$  based on the dispersion relation (13), which we have illustrated in Fig.5. Furthermore, we have checked that the probability density  $|\phi_A^{s_z}(\theta)|^2$  agrees excellently with the result obtained based on the tight-binding model in Fig.4.

## CONCLUSION

We have uncovered a salient fact of silicon nanotube that it is a topological insulator by studying its band structure in

uniform electric field  $E_z$ . When  $E_z > E_{cr}$ , there emerges four helical zero modes propagating along the nanotube. They form metallic regions separating topological and band insulators. We have constructed the wave function of each zero mode based on the effective Dirac theory. Silicon nanotube may be an ideal material to transport spin currents. It may be used as a quantum wire in future spintronics. Our results are applicable also to germanium nanotube.

## ACKNOWLEDGEMENTS

I am very much grateful to N. Nagaosa for many fruitful discussions on the subject. This work was supported in part by Grants-in-Aid for Scientific Research from the Ministry of Education, Science, Sports and Culture No. 22740196.

- 
- [1] Saito R., Dresselhaus G. Dresselhaus M. S., *Physical Properties of Carbon Nanotubes* (Imperial College Press, London) (1998)
  - [2] Ando T., J. Phys. Soc. Jpn. **74** (2005) 777
  - [3] Takeda K. Shiraishi K., Phys. Rev. B **50** (1994) 075131
  - [4] Aufray B., Vizzini A., Oughaddou H., Lndri C., Ealet B. Lay G.L., Appl. Phys. Lett. **96** (2010) 183102
  - [5] Liu C.-C., Feng W. Yao Y., Phys. Rev. Lett. **107** (2011) 076802
  - [6] Ezawa M., New J. Phys. **14** (2012) 033003
  - [7] Sha J., Niu J., Ma X., Xu J., Zhang X., Yang Q. Yang, D., Advanced Materials **14** (2002) 1219
  - [8] De Crescenzi M., Castrucci P., Scarselli M., Diociaiuti M., Chaudhari P. S., Balasubramanian C., Bhave T. M. Bhoraskar S. V., Appl. Phys. Lett. **86** (2005) 231901
  - [9] Perepichka D. F. Rosei F., Small **2** (2006) 22
  - [10] Hasan M. Z. Kane C., Rev. Mod. Phys. **82** (2010) 3045
  - [11] Qi X.-L. Zhang S.-C., Rev. Mod. Phys. **83** (2011)1057
  - [12] Wu C., Bernevig B. A. Zhang S.-C., Phys. Rev. Lett. **96** (2006) 106401
  - [13] Kane C. L. Mele E. J., Phys. Rev. Lett. **95** (2005) 226801
  - [14] Min H., Hill J. E., Sinitsyn N. A., Sahu B. R., Kleinman L. MacDonald A. H., Phys. Rev. B **74** (2006) 165310
  - [15] Yao Y., Ye F., Qi X.-L., Zhang S.-C. Fang Z., Phys. Rev. B **75** (2007) 041401
  - [16] Liu C.-C., Jiang H. Yao Y., Phys. Rev. B **84** (2011) 195430